*Oxidation of Metals, Vol. 54, Nos. 5/6, 2000*

# Oxidation Behavior and Oxide Layers of Ti–50Al Intermetallics by Preoxidation in High-Pressure Oxygen

**Mu-Rong Yang* and S. K. Wu*†**

*Received November 15, 1999; revised May 3, 2000*

*The oxidation resistance of Ti–50Al intermetallics is improved by preoxidation for 1, 4, or 16 hours in high-pressure, pure oxygen (~3.9 atm) at 900°C. Specimens preoxidized for 1 hr exhibit better oxidation resistance than others. Prolonged preoxidation time can deteriorate the oxidation resistance and reduce the parabolic-linear transition time during subsequent cyclic oxidation in 800°C air. The oxide-mound occurrence is an important factor for evaluating the effectiveness of the preoxidation treatment in oxygen. The formation mechanism of Z-phase ($Ti_5Al_3O_2$) in the Al-depleted layer beneath the flat oxide scale and that beneath the oxide mound are also proposed in this study.*

**KEY WORDS:** Ti–50Al intermetallics; preoxidation in high-pressure oxygen; cyclic-oxidation resistance; cubic Z-phase.

## INTRODUCTION

Titanium aluminide has aroused increasing interest as a light-weight, heat-resistant material intended for use in advanced gas-turbine systems of space planes and next-generation engines.[1] For years, the room-temperature brittleness and poor oxidation resistance at temperatures above 750°C have posed a bottleneck for practical applications.[1–3] Several alloying designs based on Ti–(47–48)Al (hereafter, all compositions are given in atomic percent) improved the strength and increased the tensile ductility at room temperature up to 4% elongation.[3] At the same time, in order to form a

*Institute of Materials Science and Engineering, National Taiwan University, Taipei, 106, Taiwan.
†To whom all correspondence should be addressed: e-mail: skw@ccms.ntu.edu.tw



0030-770X/00/1200-0473$18.00/0 

continuous $Al_2O_3$ layer in the oxide scale, different diffusion-barrier coating[4] and various alloying designs[5] have been pursued to enhance the high-temperature oxidation resistance of $\gamma$-TiAl alloys. However, only limited achievements have been made.

Ti–50Al does not generally form a long-lasting protective alumina scale in spite of its high aluminum content, which results in inadequate oxidation resistance. A continuous $Al_2O_3$ scale, by virtue of its slow and parabolic rate of growth, is protective and a prerequisite for attaining sufficient oxidation resistance for TiAl intermetallics. In general, the oxide scale on Ti–50Al formed in air is less protective and adherent than that formed in pure oxygen because of the detrimental effect of nitrogen.[6–8] Several reports[9–14] show that preoxidation of TiAl intermetallics at very low-pressure purified oxygen, for example, $6–8 \times 10^{-3}$ Pa, can, to some extent, successfully improve their oxidation resistance. This is because of the formation of a protective alumina-rich layer in the scale, which may come from the preferential oxidation of aluminum in low-pressure oxygen. However, the oxide scale on Ti–50Al formed by preoxidation at 950°C for 24 hr in 150 mTorr $O_2$ gas,[6] or by preoxidization at 900°C for 24 hr in 1 atm Ar + 20 vol.% $O_2$ gas is not protective against subsequent oxidation in air.[7] Obviously, the influence of oxygen pressure or preoxidation time on the oxidation resistance of preoxidized TiAl alloy is an important aspect. In addition, to the best of our knowledge, there is no report on the study of the effect of high-pressure oxygen, e.g., 3–4 atm, on the oxidation resistance of Ti–50Al.

For $\gamma$-TiAl, an Al-depleted layer forms beneath the oxide scale during oxidation in oxygen or air. Dowling and Donlon[15] found a new phase with a Ti : Al ratio of 2 : 1 in the Al-depleted layer, which results in a loss of tensile ductility at room temperature. Beye and Gronsky[16] claimed that there are two phases in the Al-depleted layer, identified as $Ti_{10}Al_6O$ and $Ti_{10}Al_6O_2$. Their subsequent study[17] indicated that there is a new phase with the composition $Ti_3Al_2O_3$ in this layer. However, recent studies indicated that there are two phases in the Al-depleted layer—one is an oxygen-interstitial solid solution of $\alpha_2$-$Ti_3Al(O)$ and the other is a new cubic phase (Z-phase) of $Ti_5Al_3O_2$ (Refs. 7, 18–21) with a space group of P432 or $P4_232$ (Refs. 7, 8, 17, 22). In a very recent study of Copland *et al.*[26] the Z-phase has a very limited composition range, indicating that Z-phase is prone to be stoichiometric. However, Dettenwanger *et al.*[23] found that the oxygen content of the Z-phase seemingly increases with increasing the oxygen concentration in an oxidizing atmosphere. Moreover, Abe *et al.*[24] considered the Z-phase to be a solid solution of oxygen in the Z-like phase in the Ti–Al system, according to the observation of the metastable Z-like phase during the early stage of crystallization of magnetron-sputtered Ti–48Al amorphous film. Hence, the characteristics of the Z-phase are still controversial.

In the present study, the preoxidation of Ti–50Al under a rather high pressure of pure oxygen was conducted and its improvement on the oxidation resistance of TiAl investigated. The possible reasons causing this improvement are discussed also.

## EXPERIMENTAL PROCEDURES

### Materials

An ingot of Ti–50Al was prepared by vacuum-arc melting followed by homogenization at 1050°C for 75 hr in vacuum. The single $\gamma$-phase, confirmed by X-ray diffraction (XRD) and metallographic observation [optimal microscopy and scanning-electron microscopy (SEM)], excluded the possibility of the presence of $\alpha_2$-$Ti_3Al$ in the ingot. Specimens in the form of coupons were cut from the ingot. Polished specimens (1-$\mu$m diamond powder) exhibited much faster oxidation kinetics in oxygen compared to ground specimens (600-grit SiC paper), which could form continuous alumina scales on the surface.[6,8,25] Hence, in order to obtain a protective alumina scale by preoxidation in this study, all the surfaces of specimen were ground by 600-grit SiC paper. Before preoxidation, the specimens were cleaned with acetone and ethanol, respectively, and finally rinsed with deionized water.

### Preoxidation Treatment

After purging with pure oxygen at least 6 times, the specimens of $15 \times 1 \times 1$ mm size (for cyclic-oxidation tests) and $8 \times 5 \times 1$ mm (for X-ray diffraction) were sealed in a quartz tube filled with 1 atm pure oxygen (99.9% industrial purity) at 27°C. The sealed quartz tube (20-mm diameter and about 250-mm length) with the specimen inside was placed in the furnace and then heated to 900°C at a heating rate of 15°C/min. In the sealed quartz tube, the volume of oxygen is much larger than that of the specimen. Therefore, the oxygen consumed in the quartz tube during the preoxidation treatment can be considered as negligible. If the volume in the quartz tube is assumed to remain constant during heating, the pressure in the quartz tube will change from 1 atm at 27°C to about 3.9 atm at 900°C according to the ideal-gas law, i.e., $PV = nRT$. The preoxidation treatment of Ti–50Al specimens used in this study was carried out in quartz tubes at 900°C for 1, 4, or 16 hr in pure oxygen at a pressure of about 3.9 atm.

### Cyclic-Oxidation Tests

The cyclic-oxidation behavior of preoxidized specimens was characterized by exposing the specimens in 800°C air in a muffle furnace and by

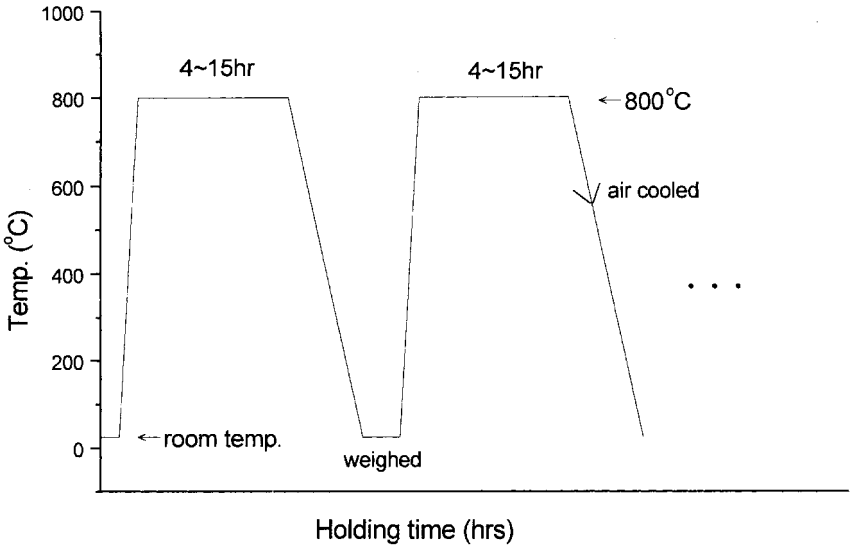


**Fig. 1.** Schematic diagram of the cyclic-oxidation test used in this study.

removing them regularly from the furnace, air cooling, weighing, and returning them to the 800°C furnace, as shown schematically in Fig. 1. The weight gains per exposed area (mg/cm$^2$), weighed on an analytical balance to an accuracy of $\pm 10^{-3}$ mg, are used to evaluate the oxidation properties.

### Microstructural Observation

The crystal structure of oxide scales was determined by XRD using a low-angle X-ray diffractometer (SIEMENS D5000) with Cu-$K_\alpha$ radiation at 45 kV, 30 mA, and a 0.03°(2$\theta$)/sec scanning rate at a grazing angle of 3°. To preserve the oxide scale during metallographic preparation, electroless nickel was plated on the oxide scale.[26] Microstructural observations were carried out by SEM with a Philips XL30, equipped with an energy-dispersive spectrometer (EDX). To discern the phases in the Al-depleted layer, some specimens used for microstructural observations were etched in Kroll's solution.

## RESULTS AND DISCUSSION

### Microstructures of the Preoxidized Specimens

After preoxidation in high-pressure oxygen at 900°C, the specimens had a grayish color. Figure 2 shows the surface morphologies of the specimens preoxidized for different times. In Fig. 2, the parallel lines on the flat

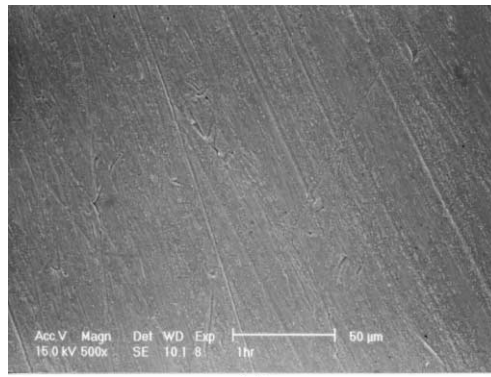


(a)

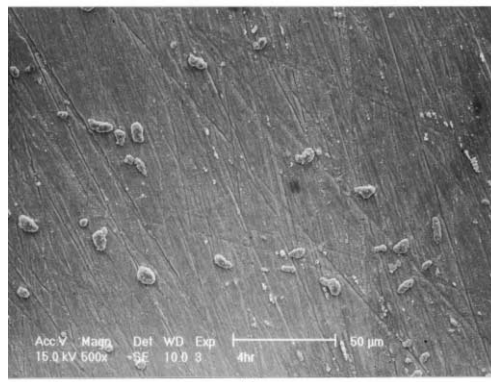


(b)

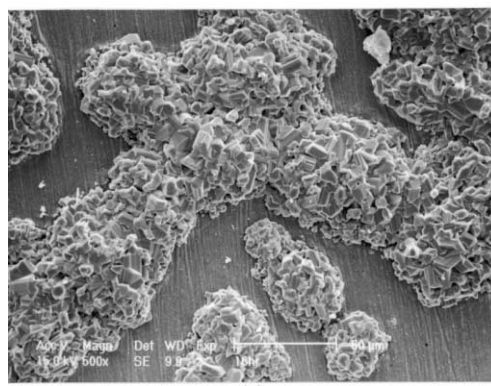


(c)

**Fig. 2.** The surface morphologies of the specimens preoxidized at 900°C high pressure oxygen for (a) 1, (b) 4, and (c) 16 hr.

surface are grinding marks, implying that the scales are very thin. No oxide mounds were found after 1-hr preoxidation, as shown in Fig. 2a. However, small oxide mounds formed on the specimen after 4-hr preoxidation and after 16-hr preoxidation formed abundant and large mounds. This feature is similar to the surface morphology of the specimen preoxidized at 1027°C for ~8.3 hr in 1 atm of Ar–1 vol.% $O_2$.[14] In Fig. 2, the oxide mounds grew in size and increased in number with increasing preoxidation time.

Figure 3 shows a cross-sectional microstructure of the oxide scale on a specimen preoxidized for 1 hr, which illustrates two uniform flat layers: an $Al_2O_3$-rich layer (~0.24 $\mu$m) and an Al-depleted layer (~0.65 $\mu$m). As the preoxidation time increased from 1 to 16 hr, the thickness of the $Al_2O_3$-rich layer and the Al-depleted layer increased from 0.24 and 0.65 $\mu$m to 0.50 and 1.26 $\mu$m, respectively. The Al-depleted layer in Fig. 3 is formed presumably because of a net outward diffusion of Al during the course of preoxidation. The opening between the oxide layer and the Ni coating results from the poor affinity of the electroless-Ni plating to the alumina-rich layer. A cross-sectional, backscattered electron (BSE) image and/or the elemental maps of oxide mounds formed on specimens preoxidized at 900°C for 4 and 16 hr are shown in Figs. 4 and 5, respectively. The microstructure of the oxide mound consists of an outer rutile-phase titania, an alumina-rich layer, and an intermixed titania/alumina layer, as shown schematically in Fig. 5e. An Al-depleted layer formed between the oxide mound and the substrate. There are some voids in the intermixed layer. By comparing Figs. 4 and 5, it can be observed that the $Al_2O_3$-rich layer in the oxide mound formed after 16 hr

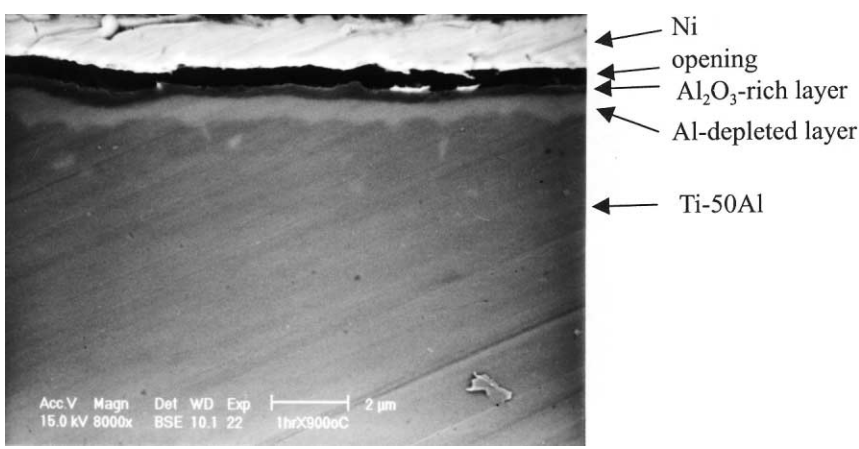


**Fig. 3.** BSE cross-sectional image of Ti–50Al preoxidized at 900°C in high-pressure oxygen for 1 hr.

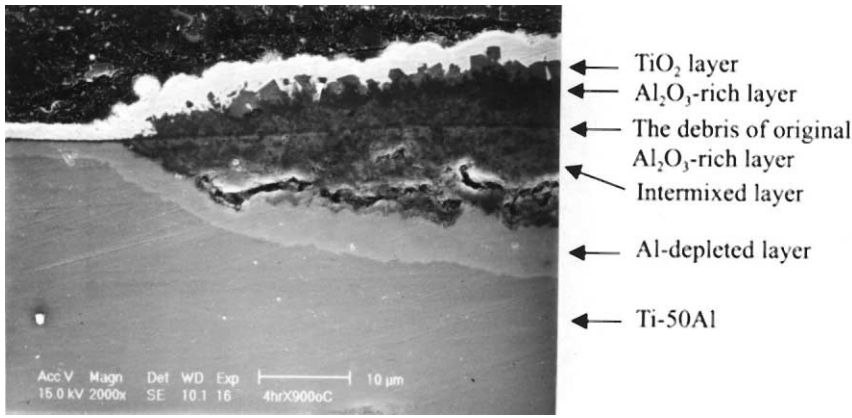


**Fig. 4.** BSE cross-sectional image of an oxide mound after preoxidation at 900°C for 4 hr in high-pressure oxygen.

preoxidation seems to be interrupted in its continuity. This may be due to the accumulated internal stress during growth of the oxide mound.[14] Careful examination of Figs. 4 and 5 shows that the debris of the flat oxide ($Al_2O_3$-rich) layer remains in the oxide mound. In this study, the linear-type, $Al_2O_3$-rich debris acts as a natural marker in the oxidation test, a feature similar to a Pt-marker test[27] in which an artificial Pt marker is intentionally positioned on the specimen. Hence, the presence of the linear $Al_2O_3$-rich debris can imply that the oxide mound on TiAl formed and grew by the simultaneous diffusion of metal (Ti and Al) and oxygen. This phenomenon also indicates that the growth rate of the oxide mound in high-pressure oxygen is faster than that formed at a reduced pressure (1 atm of He + 20% $O_2$) or at a low pressure ($6–8 \times 10^{-3}$ Pa) of oxygen. In the latter two cases, no linear-type $Al_2O_3$-rich debris is reported after preoxidation.[11,14]

## XRD Analysis of the Preoxidized Specimens

Figures 6a–c show low-angle XRD patterns of the flat oxide scale of specimens preoxidized in high-pressure oxygen for 1, 4, and 16 hr, respectively. From Fig. 6a, a minute amount of $TiO_2$ is imbedded in the $Al_2O_3$-rich layer of Fig. 3. From Figs. 6b and c it can be seen that prolonged preoxidation time increased the diffraction intensities of $Al_2O_3$ and $TiO_2$ and suppressed those of the Ti–50Al matrix ($\gamma$-TiAl). Careful examination of Fig. 6, for 1 and 4-hr preoxidized specimens, shows that there are some reflection peaks associated with $\alpha_2$-$Ti_3Al$. For all specimens, however, a number of reflection peaks can be attributed to the new cubic Z-phase with

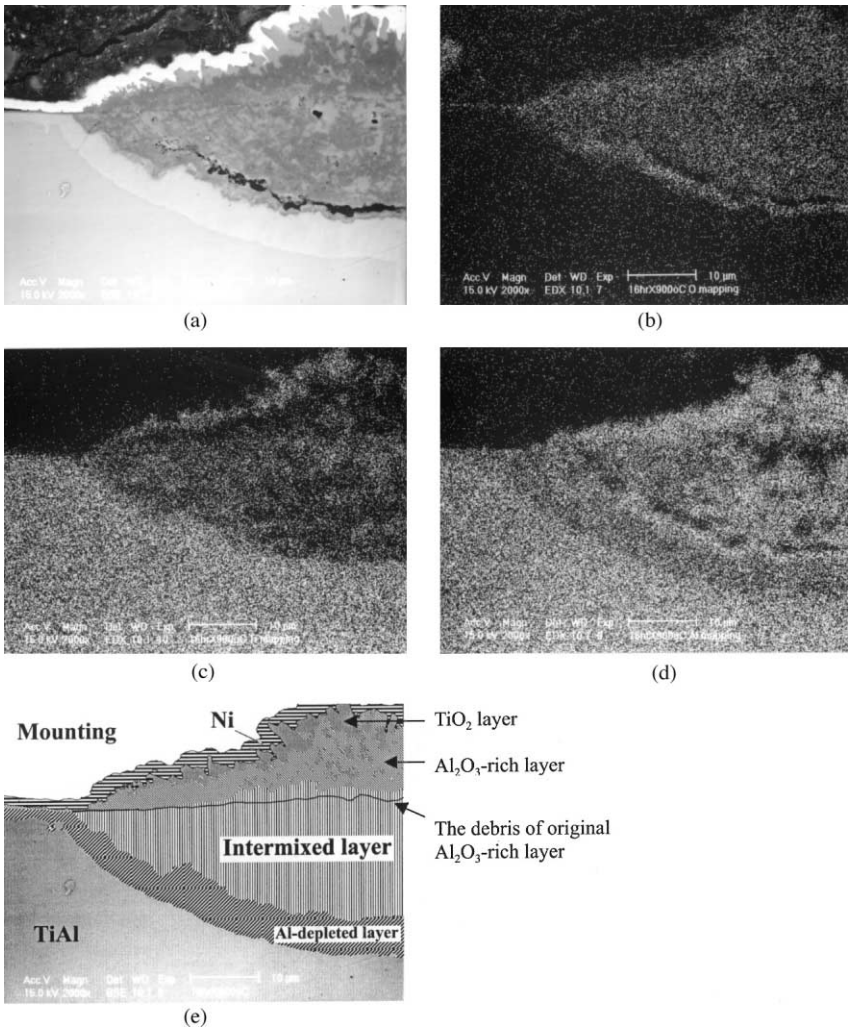


**Fig. 5.** Cross-sectional morphologies of an oxide mound after preoxidization at 900°C for 16 hr in high-pressure oxygen. (a) BSE image; (b) O map; (c) Ti map; (d) Al map, and (e) schematic diagram of the oxide mound of (a).

$a = 0.690$ nm,[7,18,19] which is not included in the JCPDS database. The composition of the Z-phase is believed to be $Ti_5Al_3O_2$ with a small homogeneity range.[18] The formation mechanism of the Z-phase in the Al-depleted layer is discussed in the next two sections.

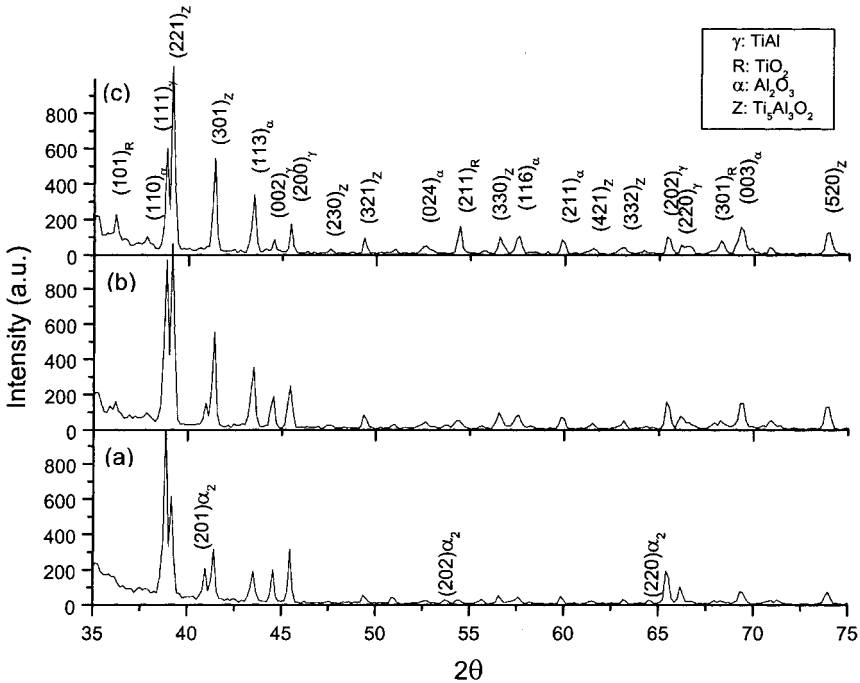


**Fig. 6.** XRD patterns of Ti–50Al specimens preoxidized at 900°C for (a) 1, (b) 4, and (c) 16 hr in high pressure oxygen.

## Formation Mechanism of the Z-Phase in the Al-Depleted Layer beneath the Flat Oxide Scale

The peak intensities of the Z-phase increase with increasing preoxidation time, as shown in Fig. 6, which is consistent with the case of oxidation at reduced oxygen pressure (1 atm of He + 20 vol.% $O_2$) as reported by Gross *et al.*[28] Nevertheless, Gross *et al.* attributed the decrease of reflection intensities of $\alpha_2$-$Ti_3Al$ with increasing preoxidation time to greater absorption of the X-ray beam by the growing scale. They demonstrated that a single Z-phase in the Al-depleted zone formed in the early period of oxidation in 1 atm of He + 20 vol.% $O_2$ at 800 or 900°C and subsequent oxidation could further consume Al and lead to the formation of $\alpha_2$-$Ti_3Al$ in the Al-depleted zone.[18,27] However, the absorption effect of XRD diffraction should have the same influence on both the peaks of Z-phase and $\alpha_2$-$Ti_3Al$, instead of those of $\alpha_2$-$Ti_3Al$ only. Hence, from the results of Fig. 6, in which the peak intensities of $\alpha_2$-$Ti_3Al$ decrease, but those of the Z-phase increase

with increasing preoxidation time, we suggest that the volume of $\alpha$-$Ti_3Al$ in the Al-depleted layer beneath the flat oxide scale should decrease with increasing preoxidation time. However, the hypothesis of Al consumption in the Al-depleted layer cannot satisfactorily explain the fact that prolonged preoxidation favors the formation of the Z-phase, instead of the formation of $\alpha_2$-$Ti_3Al$.

XRD results, as shown in Fig. 6, indicate that the initial preferential oxidation of aluminum forms the $\alpha_2$-phase adjacent to the oxides, as observed in the TEM investigation of the early stages of TiAl oxidation.[29] Since the Z-phase can be synthesized by powder-metallurgical methods,[19] the Z-phase ($Ti_5Al_3O_2$) might have formed due to the reaction of the $\alpha_2$-phase and/or $\gamma$-TiAl substrate with O and/or $Al_2O_3$. It has been reported that alumina and titania do not react with each other and are stable below 1010°C (Ref. 16). XRD analysis of a reaction couple of $Al_2O_3$ and $\alpha_2$-$Ti_3Al$ at 900°C for 100 hr reveals that only $\alpha_2$-$Ti_3Al$, $Al_2O_3$, and $\gamma$-TiAl are found.[30] The absence of Z-phase in this reaction couple has excluded the possibility of the reaction:

$$2Al_2O_3 + 5Ti_3Al \rightarrow 3Ti_5Al_3O_2$$

in the formation of Z-phase. Figure 7a shows a cross-sectional morphology of an etched specimen preoxidized for 1 hr. In Fig. 7a, the outmost layer (layer I) is $Al_2O_3$-rich. The darker area (layer II) has a lower aluminum content than the light area (layer III) from the results of EDX analyses at positions 2 and 3 of Fig. 7a, regardless of the limitation of SEM resolution. This feature is consistent with the proposal of Al depletion, i.e., preferential outward Al diffusion to form a protective $Al_2O_3$-rich layer.[7,18] We suggest that the darker (layer II) and lighter (layer III) areas are $\alpha_2$-$Ti_3Al$ and Z-phase, respectively. (The image contrast between $\alpha_2$-$Ti_3Al$ and Z-phase of Fig. 7a is in agreement with the case of the oxide mound in Fig. 7c, as discussed in the following section.)

The formation mechanism of Z-phase formed in the Al-depleted layer beneath the flat oxide scale might have resulted from the reaction among oxygen, TiAl, and $Ti_3Al$. Because $\alpha_2$-$Ti_3Al$ has a higher solubility than $\gamma$-TiAl for interstitially dissolved oxygen,[14,31] the oxygen involved in the reaction may be the inward-diffusing oxygen and/or the oxygen dissolved in $\alpha_2$-$Ti_3Al$. As mentioned above, outward Al diffusion during the course of preoxidation can induce the formation of $\alpha_2$-$Ti_3Al$. However, the inward oxygen diffusion can be limited by the outermost protective $Al_2O_3$-rich layer. This feature can reduce outward Al diffusion, which is induced by preferential oxidation of Al and, at the same time, can slow down the formation of $\alpha_2$-$Ti_3Al$. Hence, the formation reaction of Z-phase will consume the $\alpha_2$-$Ti_3Al$ and result in a decrease in reflection intensities of $\alpha_2$-$Ti_3Al$ as

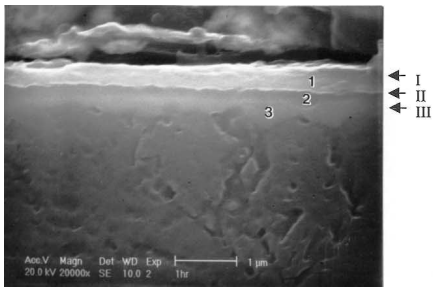


(a)

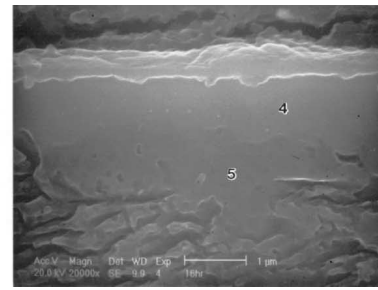


(b)

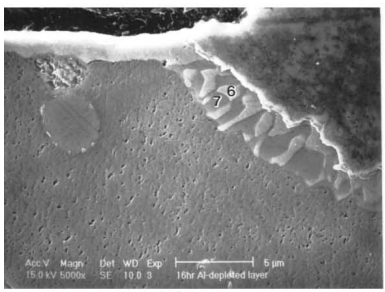


(c)

| EDX position | Ti(at.%) | Al(at.%) | O(at.%) | Suggested phase |
|---|---|---|---|---|
| 1 | 18.89 | 24.21 | 56.90 | $Al_2O_3$-rich |
| 2 | 22.66 | 27.32 | 50.02 | $\alpha_2$-$Ti_3Al$ |
| 3 | 38.12 | 30.83 | 31.05 | Z phase |
| 4 | 46.97 | 34.70 | 18.33 | Z phase |
| 5 | 45.51 | 45.73 | 8.76 | $\gamma$-TiAl |
| 6 | 52.27 | 28.20 | 19.23 | Z phase |
| 7 | 56.55 | 25.84 | 17.62 | $\alpha_2$-$Ti_3Al$ |

**Fig. 7.** Secondary-electron images and EDX analysis of the Al-depleted layer of etched specimens pre-oxidized at 900°C for (a) 1 hr and (b, c) 16 hr in high-pressure oxygen.

the preoxidation time increases. After 16-hr preoxidation, as shown in Fig. 7b, the Z-phase (lighter area, verified by EDX result of position 4) grows and $\alpha_2$-$Ti_3Al$ diminishes. This result is consistent with the XRD result of Fig. 6c and is the same as the Al-depleted zone beneath the flat oxide scale formed at reduced oxygen pressure for 24 hr.[7] The high oxygen solubility in the $\gamma$-TiAl matrix near the Al-depleted layer (EDX position 4 of Fig. 7) may result from the interaction volume of the incident electron beam and materials, which leads to the artifact of the oxygen signal contributed from the Al-depleted layer. After the amount of $\alpha_2$ decreases, the Z-phase is proposed to grow continuously if the outward Al diffusion and inward oxygen enrichment are still in progress. Obviously, the growth rate of the Z-phase should be slowed down at this point.

## Formation Mechanism of the Z-Phase in the Al-Depleted Layer beneath the Oxide Mound

The cross-sectional microstructure of an etched specimen preoxidized for 16 hr, as shown in Fig. 7c, reveals that the Al-depleted layer beneath the oxide mound consists of Z-phase (lighter area) and $\alpha_2$-$Ti_3Al$ (darker area),

as discerned and confirmed by EDX analyses at positions 6 and 7, respectively. The two-phase morphology observed in the Al-depleted layer of Fig. 7c is similar to that formed in reduced-pressure oxygen for 24 (Ref. 7) and 150 hr (Ref. 18) at 900°C. The image constrast of these two phases is also in agreement with the result of Dettenwanger *et al.*[8] The structure of the Al-depleted layer beneath the oxide mound cannot be detected by low-angle XRD (grazing angle = 3°) due to the absorption of the X-ray beam. Hence, even if there is $\alpha_2$-$Ti_3Al$ in the Al-depleted layer of Fig. 7c, no obvious peak intensities of $\alpha_2$-$Ti_3Al$ can be detected in Fig. 6c. If $\alpha_2$-$Ti_3Al$ formed from a continuous net outward Al diffusion during the course of preoxidation, $\alpha_2$-$Ti_3Al$ should be located mostly around the outer part of the Al-depleted layer (are near the oxide mound) due to the $\alpha_2$-$Ti_3Al$ having less Al than the Z-phase. However, Fig. 7c indicates that the Z-phase, instead of $\alpha_2$-$Ti_3Al$, is prone to locate around the area near the oxide mound. This feature implies that the formation mechanism of Z-phase in the Al-depleted layer beneath the flat oxide scale (discussed in the last section) cannot be used in this section. In addition, from the cross-sectional microstructures of oxide mounds of Figs. 4, 5, and 7, no internal oxidation in the Al-depleted layer occurred, i.e., no preferential oxidation of aluminum was observed. Hence the preferential oxidation of Al in the depleted zone leading to the formation of $\alpha_2$-$Ti_3Al$ cannot also be satisfactorily explained in this section. Therefore, an other possible mechanism for the formation of Z-phase observed in Fig. 7c should be proposed.

The microstructure of the Al-depleted zone observed in Fig. 7c probably results from the poor protection of the oxide mound against inward oxygen diffusion. The continuous outward Al diffusion can deplete the Al content and result in the formation of $\alpha_2$-$Ti_3Al$ near the TiAl substrate. The inward diffusion of oxygen cannot only form oxide to promote outward Al diffusion, but also react with Al and $\alpha_2$-$Ti_3Al$ to form the Z-phase near the oxide mound. Although the exact procedure of oxygen reacting with Al and $\alpha_2$-$Ti_3Al$ to form the Z-phase is unclear now, this reaction may still play an important role in the formation of the two-phase microstructure of the Al-depleted layer observed in Fig. 7c.

## Cyclic-Oxidation Kinetics

Results of cyclic oxidation performed at 800°C for the preoxidized specimens are given in Fig. 8. The as-homogenized Ti–50Al specimen without any pre-oxidation treatment is also plotted in Fig. 8. It can be seen that preoxidation in high-pressure oxygen can improve the oxidation resistance of Ti–50Al. The oxidation resistance deteriorates as the preoxidation time increases. For the as-homogenized Ti–50Al specimen cyclically oxidized at

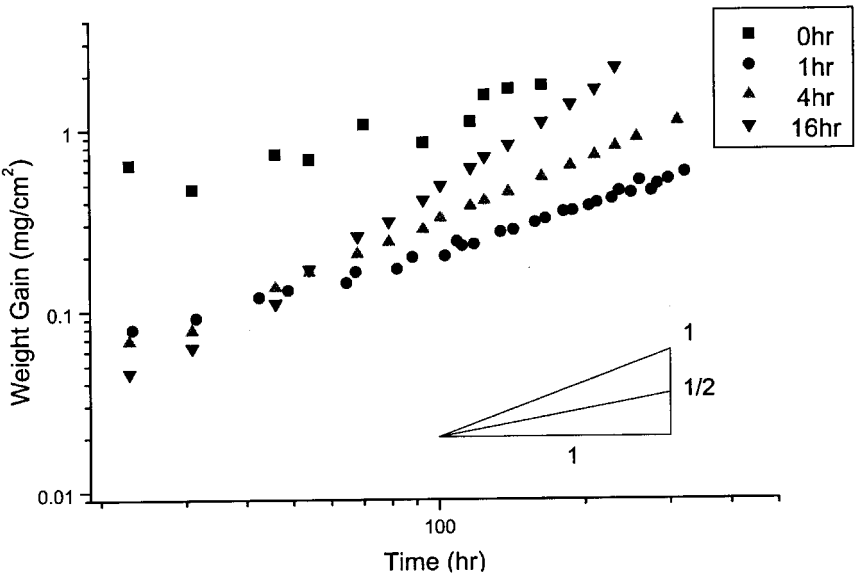


**Fig. 8.** Cyclic-oxidation weight gains vs. time in static 800°C air for specimens with and without preoxidation.

800°C, scale spallation occurs within 30-hr cyclic exposure. For the specimen preoxidized for 1 hr, no scale spallation occurs during subsequent 800°C cyclic oxidation, even if the accumulated cyclic-oxidation time exceeds more than 318 hr. The cyclic-oxidation behavior of a specimen preoxidized for 1 hr is found to shift from a parabolic rate law to a linear rate law after about 90-hr cyclic oxidation, as demonstrated by the slope from $\frac{1}{2}$ to 1 in Fig. 8, which is known as the "breakaway".[32] For a specimen preoxidized for 4 hr, breakaway occurs at about 35-hr cyclic oxidation. Since the breakaway occurs as the continuity of the stratified $Al_2O_3$-rich layer has been interrupted for the as-cast TiAl specimens oxidized in air,[33] the continuity of the $Al_2O_3$-rich layer in the oxide mound of Fig. 8 might have also been interrupted after breakaway. From Fig. 8, it can be seen that the prolonged preoxidation time can reduce the parabolic-linear transition time. The oxide mound seems to be an "Achilles heel" for the oxidation resistance of Ti–50Al.

## Microstructures of Preoxidized Specimens after Cyclic Oxidation

The surface morphologies of preoxidized specimens after 318-hr cyclic oxidation, as shown in Fig. 9, indicate that the size and the number of oxide

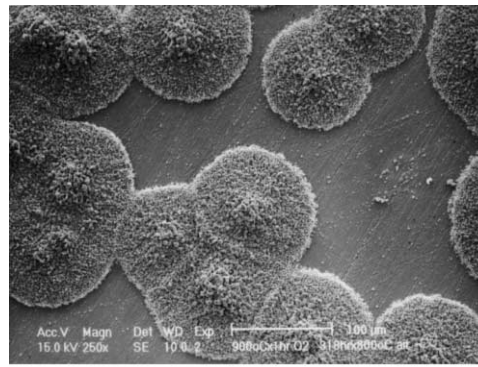


(a)

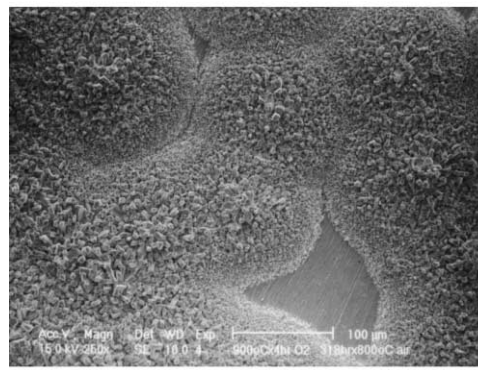


(b)

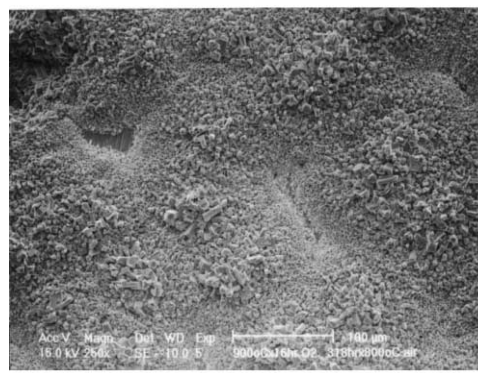


(c)

**Fig. 9.** Surface morphologies of specimens after cyclic oxidization at 800°C in air for 318 hr. The specimens were preoxidized at 900°C for (a) 1, (b) 4, and (c) 16 hr in high-pressure oxygen.

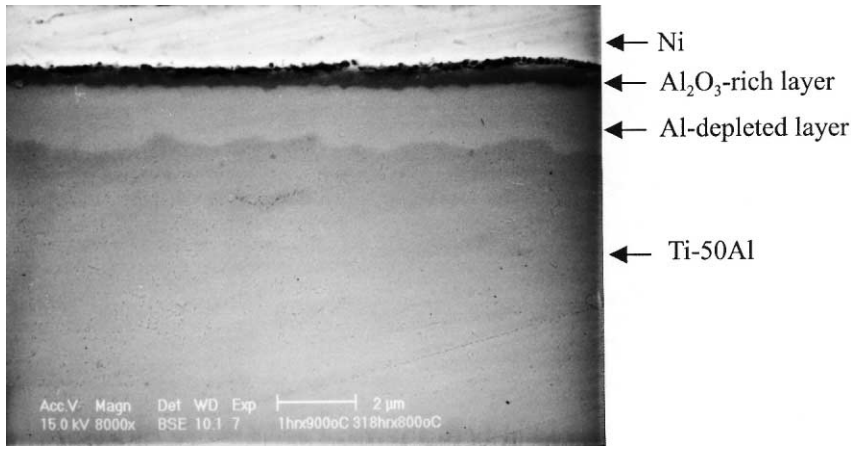


**Fig. 10.** BSE cross-sectional image of the flat oxide scale of Fig. 9a.

mounds after cyclic oxidation increase with increasing preoxidation time. The longer the preoxidation time, the more the oxide mounds cover the specimen surface after 318-hr cyclic oxidation. This trend is consistent with the result of the cyclic-oxidation curves shown in Fig. 8. However, the number of oxide mounds formed during the preoxidation does not seem to increase greatly after subsequent cyclic oxidation. Most of the oxide mounds grow and extend only laterally on the surface during the course of cyclic oxidation. The growth of oxide mounds seemingly dominates the measured overall weight gain of the cyclically-oxidized specimens.

Figure 10 shows the cross-sectional microstructure of the flat oxide scale of Fig. 9a. It indicates that the scale still consists of two layers, an $Al_2O_3$ scale (~0.40 $\mu$m) and an Al-depleted layer (~1.46 $\mu$m). The absence of $TiO_2$ sprout in Fig. 10 implies that the $Al_2O_3$-rich layer in the flat oxide scale still exhibits excellent oxidation resistance after 318-hr cyclic oxidation. Figure 11 shows the cross-sectional microstructure of Fig. 9c and indicates that the constituents of the oxide scale of Fig. 9c are similar to those of Fig. 5. This implies that the preoxidation treatment does not alter the oxidation mechanism during cyclic oxidation, but it can substantially reduce the oxidation rate, as indicated in Fig. 8.

## Effect of Oxygen Pressure and Preoxidation Time on the Oxidation-Resistance Improvement of Ti–50Al Alloy

According to Fig. 8, Ti–50Al intermetallics preoxidized in high-pressure oxygen can reduce the cyclic-oxidation rate. The improvement can be

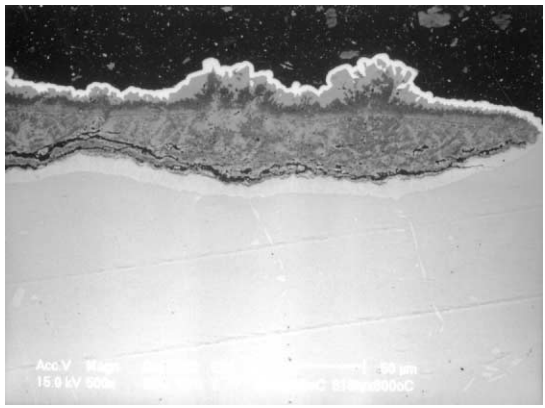

**Fig. 11.** BSE cross-sectional image of the oxide mounds of Fig. 9c.

attributed to the formation of a protective $Al_2O_3$-rich layer as the parabolic rate law holds. However, the parabolic rate law fails if the continuity of the $Al_2O_3$-rich layer is disrupted by oxide mounds. The failure of improved oxidation resistance after preoxidation at 900°C for 24 hr in 1 atm Ar + 20 vol.% $O_2$ gas[7] may not be associated with the insufficient amount of oxygen at low pressures. However, the long preoxidation time (24 hr) results in the formation of porous oxide mounds, which can facilitate the diffusion of oxidizing species to accelerate oxidation. Preoxidation in pure oxygen at high pressure (3–4 atm), is also a feasible method for improving the oxidation resistance of Ti–50Al intermetallics. In addition to the factor of oxygen pressure, we find that the influence of preoxidation time on the oxide-mound appearance is most important for evaluating the effectiveness of preoxidation treatments.

## CONCLUSIONS

The oxidation resistance of Ti–50Al intermetallics is improved by preoxidation for different times (1, 4, or 16 hr) in high-pressure (~3.9 atm) oxygen at 900°C. The oxide mounds increased in number and size with increasing preoxidation time. The structure of the oxide mound consists of an outer rutile-phae titania, an alumina-rich layer, and an intermixed titania–alumina layer. An Al-depleted layer formed beneath both the flat oxide scale and the oxide mound. The amount of Z-phase ($Ti_5Al_3O_2$) in the Al-depleted layer beneath the flat oxide layer increases with increasing preoxidation time by the reaction of oxygen, TiAl, and $Ti_3Al$. For the Al-depleted layer beneath the oxide mound, a two-phase microstructure of $\alpha_2$-$Ti_3Al$ and

Z-phase is observed. Here the $\alpha_2$-$Ti_3Al$ is located at the site near the TiAl substrate. Specimens preoxidized for 1 hr at high-pressure oxygen exhibit good cyclic-oxidation resistance. Prolonged preoxidation time can deteriorate the oxidation resistance and reduce the parabolic-linear transition time during subsequent cyclic oxidation in 800°C air. In this study, we found that preoxidation in high-pressure oxygen can be used to improve the oxidation resistance. Oxide-mound occurrence is an important factor for evaluating the effectiveness of preoxidation treatments in pure oxygen.

## ACKNOWLEDGMENTS

The authors are indebted to Dr. Shu-Chiao Tsai for his assistance in the experimental work. The authors are also pleased to acknowledge the financial support of this research by the National Science Council (NSC), Republic of China, under the Grant NSC88-2216-E002-026.

## REFERENCES

1. D. M. Dimiduk, D. B. Miracle, and C. H. Ward, *Mater. Sci. Technol.* **8**, 367 (1992).
2. T. Shimizu, T. Iikubo, and S. Isobe, *Mater. Sci. Eng.* **A153**, 602 (1992).
3. Y. W. Kim, *JOM* **41**, 30 (1994).
4. X. Dong, Z. Zhihong, L. Xianghuai, Z. Shichang, S. Taniguchi, T. Shibata, and T. Yamada, *Surf. Coat. Technol.* **66**, 486 (1994).
5. M. P. Brady, W. J. Brindley, J. L. Smialek, and I. E. Locci, *JOM* **48**, 46 (1996).
6. S. Choudhury, H. C. Graham, and J. W. Hinze, *Proceedings of the Symposium on Properties of High Temperature Alloys* (The Electrochemical Society, Princeton, NJ, 1976), p. 668.
7. N. Zheng, W. J. Quadakkers, A. Gil, and H. Nickel, *Oxid. Met.* **44**, 477 (1995).
8. F. Dettenwanger, E. Schumann, M. Rühle, J. Rakowski, and G. H. Meier, *Oxid. Met.* **50**, 269 (1998).
9. E. Kobayashi, M. Yoshihara, and R. Tanaka, *High Temp. Technol.* **8**, 179 (1990).
10. M. Yoshihara, T. Suzuki, and R. Tanaka, *ISIJ Intern.* **31**, 1201 (1991).
11. S. Taniguchi, T. Shibata, and A. Murakami, *Oxid. Met.* **41**, 103 (1994).
12. S. Taniguchi, T. Shibata, A. Murakami, and K. Chihara, *Oxid. Met.* **42**, 17 (1994).
13. S. Taniguchi, T. Shibata, and S. Sakon, *Mater. Sci. Eng.* **198A**, 85 (1995).
14. S. Taniguchi, Y. Tachikawa, and T. Shibata, *Mater. Sci. Eng.* **232A**, 47 (1997).
15. W. E. Dowling, Jr. and W. T. Donlon, *Scripta Metall. Mater.* **27**, 1663 (1992).
16. R. W. Beye and R. Gronsky, *Acta Metall. Mater.* **42**, 1373 (1994).
17. R. Beye, M. Verwerft, J. T. M. De Hosson, and R. Gronsky, *Acta Mater.* **44**, 4225 (1996).
18. N. Zheng, W. Fischer, H. Grübmeier, V. Shemet, and W. J. Quadakkers, *Scripta Metall. Mater.* **33**, 47 (1995).
19. V. Shemet, P. Karduck, H. Hoven, B. Grushko, W. Fischer, and W. J. Quadakkers, *Intermetallics* **5**, 271 (1997).
20. E. H. Copland, B. Gleeson, and D. J. Young, *Acta Mater.* **47**, 2937 (1999).
21. V. Shemet, H. Hoven, and W. J. Quadakkers, *Intermetallics* **5**, 311 (1997).
22. Y. F. Cheng, F. Dettenwanger, J. Mayer, E. Schumann, and M. Rühle, *Scripta Metall. Mater.* **34**, 707 (1996).
23. F. Dettenwanger, E. Schumann, J. Rakowski, G. H. Meier, and M. Rühle, *Mater. Corros.* **48**, 23 (1996).
24. E. Abe, M. Ohnuma, and M. Nakamura, *Acta Mater.* **47**, 3607 (1999).

25. J. M. Rakowski, G. H. Meier, F. S. Pettit, F. Dettenwanger, E. Schumann, and M. Rühle, *Scripta Metall. Mater*. **35**, 1417 (1996).
26. G. E. Co., U.S. patent 4,780,342, Oct. 25, 1988.
27. B. G. Kim, G. M. Kim, and C. J. Kim, *Scripta Metall. Mater*. **33**, 1117 (1995).
28. M. Gross, V. Kolarik, and A. Rahmel, *Oxid. Met*. **48**, 171 (1997).
29. C. Lang and M. Schütze, *Oxid. Met*. **46**, 255 (1996).
30. A. K. Misra, *Metall. Trans*. **22A**, 715 (1991).
31. X. L. Li, R. Hillel, F. Teyssandier, S. K. Choi, and F. J. van Loo, *Acta Metall. Mater*. **40**, 3149 (1992).
32. Y. Shida and H. Anada, *Mater. Trans. JIM* **34**, 236 (1993).
33. M. Schmitz-Niederau and M. Schütze, *Oxid. Met*. **52**, 225 (1999).